RKDG methods with WENO limiters for unsteady cavitating flow

Jun Zhu [a,b], Tiegang Liu [c], Jianxian Qiu [d], Boo Cheong Khoo [a,e,*]

[a] Singapore-MIT Alliance, 4 Engineering Drive 3, National University of Singapore, Singapore 117576, Singapore
[b] College of Science, Nanjing University of Aeronautics and Astronautics, Nanjing, Jiangsu 210016, PR China
[c] LMIB and School of Mathematics and System Sciences, Beijing University of Aeronautics and Astronautics, Beijing 100191, PR China
[d] School of Mathematical Sciences, Xiamen University, Xiamen, Fujian 361005, PR China
[e] Department of Mechanical Engineering, National University of Singapore, Singapore 119260, Singapore

ARTICLE INFO

ABSTRACT

In this paper, we develop the Runge–Kutta discontinuous Galerkin (RKDG) methods with the finite volume weighted essentially non-oscillatory (WENO) reconstruction as limiters to solve for the unsteady cavitating flow under the employment of the isentropic one-fluid model. To treat the cavitating flow and suppress the possible spurious oscillations in the vicinity of the cavitation boundary, the TVB limiter is used as an indicator to detect the "troubled cells" and hence take the advantage of utilizing the WENO reconstruction for the freedoms of the RKDG methods. Numerical results are provided to illustrate the viability of these procedures.

© 2011 Elsevier Ltd. All rights reserved.

1. Introduction

The dynamics of fluid flow is very important in many fields, one of which is the occurrence of cavitation when the pressure in the liquid (such as water) drops below the saturated vapor pressure. A typical example is the flow generated by an underwater explosion near a structure or a free surface. The cavitating flow very often follows such progression: cavitation creation, evolution and finally collapse. To date, there is no single model that can be applied to simulate all kinds of cavitation. In general, there are two different approaches to the cavitation modeling: one is the two-fluid model and the other is the one-fluid model. The methodology of the two-fluid model assumes both phases co-exist at every location of the flow field and each phase is governed by its specific partial differential equations (PDEs). One of the representative work is that carried out by Saurel et al. [18]. The one-fluid model treats the cavitating flow as a mixture of two fluids behaving as one. As such, only one set of PDEs similar to the single phase flow is used to govern the whole fluid region. A baro-tropic or homogeneous assumption [2] can be used to develop a reasonable constitutive relationships of liquid, vapor and the mixture medium [11,19,23,25]. The interest of this work lies in the unsteady (transient) cavitation caused by the pressure jump across the cavitation boundary. Such unsteady cavitation is commonly observed in the underwater explosion, where both the ambient liquid and the mixture have to be considered as compressible. For the simulation of such cavitation, the isentropic one-fluid model [11] is employed. Besides the modeling of cavitation, there are other numerical difficulties encountered in simulation. One of the dominant difficulty is the need to suppress unwanted/unnatural numerical oscillations. Due to the existence of cavitation interface, numerical oscillations usually occur at the interfacial region similar to that found in the simulation of multi-material flow.

In this work, we intend to take the advantage of the weighted essentially non-oscillatory (WENO) reconstruction to overcome the numerical oscillations occurring in the vicinity of cavitation boundary. The technique of WENO reconstruction was originally proposed by Qiu et al. [15,29] as a limiter to eliminate the numerical oscillations which occur in the discontinuous Galerkin (DG) methods. The DG methods was first introduced by Reed and Hill

in 1973 in the context of neutron transport (steady state linear hyperbolic equations) [17] and experienced a major development in 1990s due to Cockburn and Shu [4–8]. One of the more popular version of DG proposed by Cockburn and Shu is an explicit, nonlinearly stable high order Runge–Kutta time discretizations [22] and DG discretization in space with an exact or approximate Riemann solver as interface fluxes and total variation bounded (TVB) limiter [20] to achieve non-oscillatory properties for strong shocks. These schemes have been famously termed as RKDG methods. An important component of a RKDG method for solving conservation laws with strong shocks is the employment of nonlinear limiter. There are various limiters developed in the literature, and can be categorized as the TVB limiters [4–8], the moment based limiters [1,3] and the WENO reconstruction based limiters [15,29,13,14,16,26–28]. Among them, the WENO reconstruction based limiters are capable of ensuring consistent accuracy. One major advantage of the RKDG methods over the finite difference schemes is their compactness and convenience of implementation to achieve higher order of numerical accuracy.

The RKDG methods have been very successful in applications for single phase flow. On the other hand, there is much less work related to the RKDG methods as applied to the multiphase flow and in particular unsteady cavitation flow. In this work, our interest is to develop the RKDG methods to simulate the compressible unsteady cavitating flow by taking advantage of the weighted essentially non-oscillatory (WENO) reconstruction. Because large density jump and fluid properties change occur across the cavitation interface, it is expected that the major difficulty may come from the treatment of the cavitation mixture when the RKDG approach is employed to simulate the cavitation flow. Firstly, one has to identify the cavitation mixture. Secondly, one has to construct a limiter procedure to suppress the numerical oscillations occurring in the region of cavitation. Lastly, one needs to obtain the flow state in the region of cavitation. To overcome the above-mentioned difficulties, it is thought appropriate that we treat the cavitation as a "troubled" region. With this treatment, one will find that the RKDG with the WENO reconstruction based limiter works specially well to simulate the cavitation flow constituted with a one-fluid model.

The organization of this paper is as follows: in Section 2, we briefly review and construct the finite volume WENO schemes as limiters for the RKDG methods with the isentropic one-fluid model as the cavitation EOS (Equation-of-State) in one and two dimensions. Several one and two dimensional numerical tests for the unsteady cavitation phenomena are found in Section 3 for verification and study of the associated flow dynamics. Concluding remarks are given in Section 4.

2. WENO schemes as limiters for the RKDG methods with isentropic one-fluid model simulation

In this section, we firstly consider the one dimensional system:

$$\frac{\partial}{\partial t}\begin{pmatrix} \rho \\ \rho u \end{pmatrix} + \frac{\partial}{\partial x}\begin{pmatrix} \rho u \\ \rho u^2 + p \end{pmatrix} = 0, \tag{2.1}$$

which can be rewritten as

$$\frac{\partial U}{\partial t} + \frac{\partial F(U)}{\partial x} = 0. \tag{2.2}$$

Next, we consider the two dimensional system:

$$\frac{\partial}{\partial t}\begin{pmatrix} \rho \\ \rho u \\ \rho v \end{pmatrix} + \frac{\partial}{\partial x}\begin{pmatrix} \rho u \\ \rho u^2 + p \\ \rho u v \end{pmatrix} + \frac{\partial}{\partial r}\begin{pmatrix} \rho v \\ \rho u v \\ \rho v^2 + p \end{pmatrix} = -\frac{n-1}{r}\begin{pmatrix} \rho v \\ \rho u v \\ \rho v^2 \end{pmatrix}, \tag{2.3}$$

and rewrite it as:

$$\frac{\partial U}{\partial t} + \frac{\partial F(U)}{\partial x} + \frac{\partial G(U)}{\partial r} = S(U). \tag{2.4}$$

Here, $\rho = \alpha\rho_g + (1-\alpha)\rho_l$ is the averaged density, ρ_l is the pure liquid density, ρ_g is the pure vapor density and the parameter $\alpha \in [0, 1]$ is the void fraction, u and v are the averaged velocities in the x- and r-directions, respectively, and p is the averaged pressure. In this paper, n is set to 2 which is applicable for a 2D axisymmetric flow. For closure of the system, the EOS is required. In the mixture, the vapor component is assumed as homogeneous, isentropic and compressible. For the pure vaporous medium, we have

$$\frac{p}{p_0} = \left(\frac{\rho_g}{\rho_{g0}}\right)^{\gamma}, \tag{2.5}$$

with $\gamma = 1.4$ and ρ_{g0} being the vapor density at the pressure p_0. We shall assume the liquid medium and the liquid component in the cavitation mixture to be compressible and isentropic. The Tait's EOS used for the water medium [9,12] is expressed as:

$$p = B\left(\frac{\rho_l}{\rho_{l0}}\right)^N - B + A, \tag{2.6}$$

$$\frac{\bar{p}}{\bar{p}_0} = \left(\frac{\rho_l}{\rho_{l0}}\right)^N, \tag{2.7}$$

where $N = 7.15$, $A = 10^5$ Pa, $B = 3.31 \times 10^8$ Pa, $p_0 = A$ and $\rho_{l0} = 1000$ kg/m³ are the initial pressure and density for the liquid, $\bar{p} = p + \bar{B}, \bar{p}_0 = p_0 + \bar{B}$ and $\bar{B} = B - A$. The sound speeds associated with pure vapor and liquid can be expressed as:

$$a_g = \left(\frac{dp}{d\rho_g}\right)^{1/2} = \left(\gamma\frac{p}{\rho_g}\right)^{1/2}, \tag{2.8}$$

and

$$a_l = \left(\frac{dp}{d\rho_l}\right)^{1/2} = \left(N\frac{\bar{p}}{\rho_l}\right)^{1/2}. \tag{2.9}$$

In this paper, we shall use the isentropic one-fluid model as EOS for the vapor–liquid mixture and described briefly below.

2.1. Isentropic one-fluid model for the cavitation region

In the isentropic one-fluid model [11], the cavitating flow is assumed to be homogenous mixture consisting of isentropic vapor and liquid components under kinematic and dynamic equilibrium with the neglect of heat transfer. The evolution of cavitation is further assumed to be driven by pressure drop across the cavitation interface. In this cavitation model, under the homogeneous, isentropic and compressible assumptions, the sound speed can theoretically be given [24] as:

$$a = \left\{[\alpha\rho_g + (1-\alpha)\rho_l]\left[\frac{\alpha}{\rho_g a_g^2} + \frac{1-\alpha}{\rho_l a_l^2}\right]\right\}^{-1/2}. \tag{2.10}$$

By the assumption of cavitation evolution driven by pressure drop alone, the void fraction $\alpha \in [0, 1]$ was derived and governed by [11]:

$$\frac{d\alpha}{dp} = \alpha(1-\alpha)\left(\frac{1}{\rho_l a_l^2} - \frac{1}{\rho_g a_g^2}\right). \tag{2.11}$$

Since the vapor and liquid components are assumed to maintain the isentropic property, the above Eqs. (2.10) and (2.11) can be integrated as:

$$\frac{\alpha}{1-\alpha} = k\frac{\left(\frac{\bar{p}}{\bar{p}_{cav}}\right)^{1/N}}{\left(\frac{p}{p_{cav}}\right)^{1/\gamma}}, \tag{2.12}$$

and

$$\rho = \frac{k\rho_g^{cav} + \rho_l^{cav}}{\left(\frac{\bar{p}}{\bar{p}_{cav}}\right)^{-1/N} + k\left(\frac{p}{p_{cav}}\right)^{-1/\gamma}}, \tag{2.13}$$

where $\bar{p} = p + B - A$ and $\bar{p}_{cav} = p_{cav} + B - A$. (2.13) is the density for the cavitating mixture, and (2.12) is the void fraction formula for the mass transfer and is directly related to the local pressure. Here $k = \frac{\alpha_0}{1-\alpha_0}$ is a model parameter and can be determined by the procedure developed in [11]. ρ_g^{cav} and ρ_l^{cav} are the associated vapor and liquid densities at the cavitation pressure p_{cav}. The overall EOS for the vapor–liquid mixture flow can then be summarised as:

$$\rho = \begin{cases} \rho_0\left(\frac{\bar{p}}{\bar{p}_0}\right)^{1/N}, & p > p_{sat}, \\ \frac{k\rho_g^{cav}+\rho_l^{cav}}{\left(\frac{\bar{p}}{\bar{p}_{cav}}\right)^{-1/N}+k\left(\frac{p}{p_{cav}}\right)^{-1/\gamma}}, & p \leqslant p_{sat}, \end{cases} \tag{2.14}$$

and

$$\frac{\alpha}{1-\alpha} = k\frac{\left(\frac{\bar{p}}{\bar{p}_{cav}}\right)^{1/N}}{\left(\frac{p}{p_{cav}}\right)^{1/\gamma}}. \tag{2.15}$$

Under the conditions in the absence of large pressure variation in the flow field, the liquid is sometimes assumed to be isothermal (as apposed to isentropic) and the sound speed for the surrounding flow is taken as a constant. The EOS for the liquid is $p - p_0 = a_l^2(\rho_l - \rho_{l0})$ instead of Tait's EOS, where ρ_{l0} is the liquid density at the pressure p_0. Therefore, the following EOS equations for the cavitation flow are obtained as:

$$\rho = \frac{k\rho_g^{cav} + \rho_l^{cav}}{\frac{p_{cav}+B'}{p+B'} + k\left(\frac{p}{p_{cav}}\right)^{-1/\gamma}}, \tag{2.16}$$

and

$$\frac{\alpha}{1-\alpha} = k\frac{\frac{p+B'}{p_{cav}+B'}}{\left(\frac{p}{p_{cav}}\right)^{1/\gamma}}, \tag{2.17}$$

where $B' = \rho_{l0}a_l^2 - p_0$. As such, the final EOS for the isothermal vapor–liquid flow mixture can be written as:

$$\rho = \begin{cases} \rho_0\left(\frac{p+B'}{p_0+B'}\right), & p > p_{sat}, \\ \frac{k\rho_g^{cav}+\rho_l^{cav}}{\left(\frac{p+B'}{p_{cav}+B'}\right)^{-1}+k\left(\frac{p}{p_{cav}}\right)^{-1/\gamma}}, & p \leqslant p_{sat}, \end{cases} \tag{2.18}$$

and

$$\frac{\alpha}{1-\alpha} = k\frac{\frac{p+B'}{p_{cav}+B'}}{\left(\frac{p}{p_{cav}}\right)^{1/\gamma}}. \tag{2.19}$$

The isentropic one-fluid model has been shown to work well. One may refer to [11] for the discussions and validations of this model.

2.2. Description of DG methods

For one dimensional cases, we shall assume that the mesh is uniformly distributed and denote the cell I_i as $I_i = [x_{i-1/2}, x_{i+1/2}]$, with the cell size $x_{i+1/2} - x_{i-1/2} = \Delta x = h$, cell centers $x_i = \frac{1}{2}(x_{i+1/2} + x_{i-1/2})$. We denote the cell averaged conservative varible U as: $\bar{U}_i(t) = \frac{1}{h}\int_{I_i} U(x,t)dx$. The space of DG solution as well as test function is given by $V_h^k = \{p : p|_{I_i} \in P^k(I_i)\}$, which is a polynomial space of degree at most k on the cell I_i. We adopt a local orthogonal basis over I_i, $\left\{\Phi_l^{(i)}(x), (l = 0, 1, \ldots, k)\right\}$, such as: $\Phi_0^{(i)}(x) = 1, \Phi_1^{(i)}(x) = \frac{x-x_i}{h}, \Phi_2^{(i)}(x) = \left(\frac{x-x_i}{h}\right)^2 - \frac{1}{12}, \ldots$. Then the numerical solution $U^h(x,t)$ of U in the space V_h^k can be written as $U^h(x,t) = \sum_{l=0}^k U_i^{(l)}(t)\Phi_l^{(i)}(x)$, for $x \in I_i$ and the degrees of freedom $U_i^{(l)}(t)$ are the moments defined by $U_i^{(l)}(t) = \frac{1}{\int_{I_i}\left(\Phi_l^{(i)}(x)\right)^2 dx}\int_{I_i} U^h(x,t)\Phi_l^{(i)}(x)dx, (l = 0, \ldots, k)$. In order to determine the approximate solution, we evolve the degrees of freedom $U_i^{(l)}(t)$:

$$\begin{aligned}
\frac{d}{dt}U_i^{(l)}(t) = &-\frac{1}{\int_{I_i}\left(\Phi_l^{(i)}(x)\right)^2 dx}\left(-\int_{I_i} F(U^h(x,t))\frac{d}{dx}\Phi_l^{(i)}(x)dx\right. \\
&+ \widehat{F}\left(U_{i+1/2}^-, U_{i+1/2}^+\right)\Phi_l^{(i)}(x_{i+1/2}) \\
&\left. - \widehat{F}\left(U_{i-1/2}^-, U_{i-1/2}^+\right)\Phi_l^{(i)}(x_{i-1/2})\right), \quad (l = 0, \ldots, k), \tag{2.20}
\end{aligned}$$

where $U_{i+1/2}^\pm = U^h(x_{i+1/2}^\pm, t)$ are the left and right limits of the discontinuous solution $U^h(x,t)$ at the cell interface $x_{i+1/2}$, $\widehat{F}(U^-, U^+)$ is a monotone flux for the scalar case and an exact or approximate Riemann solver for the system. For simplicity, we shall denote $U_i^{(*)} = U_i^{(*)}(t)$ in the following text.

When there are shock waves, numerical oscillations generally occur for the method given in (2.20). A special procedure or treatment to restrain the oscillations via say a limiter has to be incorporated into the method. The limiter adopted here is described below in some details:

$$U_{i+1/2} - = U_i^{(0)} + \widetilde{U}_i = U_i^{(0)} + \sum_{l=1}^k U_i^{(l)}\Phi_l^{(i)}(x_{i+1/2}), \tag{2.21}$$

$$U_{i-1/2}^+ = U_i^{(0)} - \widetilde{\widetilde{U}}_i = U_i^{(0)} - \left(-\sum_{l=1}^k U_i^{(l)}\Phi_l^{(i)}(x_{i-1/2})\right). \tag{2.22}$$

These are modified by the standard minmod limiter:

$$\widetilde{U}_i^{(mod)} = m\left(\widetilde{U}_i, \Delta_+ U_i^{(0)}, \Delta_- U_i^{(0)}\right), \qquad \widetilde{\widetilde{U}}_i^{(mod)} = m\left(\widetilde{\widetilde{U}}_i, \Delta_+ U_i^{(0)}, \Delta_- U_i^{(0)}\right),$$

where m is given by

$$m(a_1, \cdots, a_n) = \begin{cases} s \cdot \min_{1\leqslant j\leqslant n}|a_j|, & if \ sign(a_1) = \cdots = sign(a_n) = s, \\ 0, & otherwise, \end{cases} \tag{2.23}$$

or the TVB modified minmod function:

$$\tilde{m}(a_1, \ldots, a_n) = \begin{cases} a_1, & if \ |a_1| \leqslant M\Delta x^2, \\ m(a_1, \cdots, a_n), & otherwise, \end{cases} \tag{2.24}$$

where $M > 0$ is a constant. The choice of M depends on the problem. For scalar problem, it is possible to estimate M by the initial condition where it is proportional to the second derivative of the initial condition at smooth extrema; however, it is more difficult to estimate M for the system. If M is chosen to be too small, accuracy may degenerate at smooth extrema of the solution; if M is chosen as too large, oscillations will appear.

In this paper, we also use the limiter described above to identify the "troubled cells", namely, if one of the minmod functions gets enacted (returns other than the first argument), this cell is declared "troubled" and marked for further reconstruction. Once a "troubled cell" is identified, the WENO reconstruction to the numerical solution is made under the maintenance of conservation and accuracy. This is done via reconstructing the polynomial solutions while retaining their cell averages. With the properties of WENO reconstructions for the "troubled cells", it is much less crucial to choose an accurate M.

For two dimensional cases, we again assume that the mesh is uniformly distributed and denote the cell I_{ij} as $I_{ij} = [x_{i-1/2}, x_{i+1/2}] \times [r_{j-1/2}, r_{j+1/2}]$, with the cell size $x_{i+1/2} - x_{i-1/2} = \Delta x = h$, $r_{j+1/2} - r_{j-1/2} = \Delta r = h$ and cell centers $(x_i, r_j) = (\frac{1}{2}(x_{i+1/2} + x_{i-1/2}), \frac{1}{2}(r_{j+1/2} + r_{j-1/2}))$. We now give the test function space $V_h^k = \{p : p|_{I_{ij}} \in P^k(I_{ij})\}$ as the polynomial spaces of degree of at most k on the cell I_{ij}. We adopt a local orthogonal basis over I_{ij}, $\{\Phi_l^{(ij)}(x, r), l = 0, 1, \ldots, K;$ $K = \frac{1}{2}(k+1)(k+2) - 1\}$, such as: $\Phi_0^{(ij)}(x, r) = 1$, $\Phi_1^{(ij)}(x, r) = \frac{x - x_i}{h}$, $\Phi_2^{(ij)}(x, r) = \frac{r - r_j}{h}$, $\Phi_3^{(ij)}(x, r) = (\frac{x - x_i}{h})^2 - \frac{1}{12}$, $\Phi_4^{(ij)}(x, r) = \frac{(x - x_i)(r - r_j)}{h^2}$, $\Phi_5^{(ij)}(x, r) = (\frac{r - r_j}{h})^2 - \frac{1}{12}, \ldots$. Then the numerical solution $U^h(x, r, t)$ of U in the space V_h^k can be written as $U^h(x, r, t) = \sum_{l=0}^{K} U_{ij}^{(l)}(t) \Phi_l^{(ij)}(x, r)$, for $(x, r) \in I_{ij}$ and the degrees of freedom $U_{ij}^{(l)}(t)$ are the moments defined by $U_{ij}^{(l)}(t) = \frac{1}{\int_{I_{ij}} (\Phi_l^{(ij)}(x, r))^2 \, dx \, dr} \int_{I_{ij}} U^h(x, r, t) \Phi_l^{(ij)}(x, r) \, dx \, dr$, $(l = 0, \ldots, K)$. In order to determine the approximate solution, we evolve the degrees of freedom $U_{ij}^{(l)}(t)$:

$$\frac{d}{dt} U_{ij}^{(l)}(t) = -\frac{1}{\int_{I_{ij}} (\Phi_l^{(ij)}(x, r))^2 \, dx \, dr} \left(-\int_{I_{ij}} F(U^h(x, r, t)) \frac{\partial}{\partial x} \Phi_l^{(ij)}(x, r) \, dx \, dr \right.$$
$$- \int_{I_{ij}} G(U^h(x, r, t)) \frac{\partial}{\partial r} \Phi_l^{(ij)}(x, r) \, dx \, dr + \int_{r_{j-1/2}}^{r_{j+1/2}} \left(F(U^h(x_{i+1/2}, r, t) \Phi_l^{(ij)}(x_{i+1/2}, r)) \right.$$
$$- F\left(U^h(x_{i-1/2}, r, t) \Phi_l^{(ij)}(x_{i-1/2}, r) \right) dr$$
$$+ \int_{x_{i-1/2}}^{x_{i+1/2}} G\left(U^h(x, r_{j+1/2}, t) \Phi_l^{(ij)}(x, r_{j+1/2}) \right)$$
$$- G(U^h(x, r_{j-1/2}, t) \Phi_l^{(ij)}(x, r_{j-1/2})) \, dx$$
$$\left. - \int_{I_{ij}} S(U^h(x, r, t)) \Phi_l^{(ij)}(x, r) \, dx \, dr \right), \quad (l = 0, \ldots, K). \quad (2.25)$$

The semi-discrete schemes (2.20) and (2.25) are discretized in time by a nonlinearly stable Runge–Kutta time discretization [21]. For example, the second order version:

$$\begin{cases} U^{(1)} = U^n + \Delta t L(U^n), \\ U^{n+1} = \frac{1}{2} U^n + \frac{1}{2} U^{(1)} + \frac{1}{2} \Delta t L(U^{(1)}). \end{cases} \quad (2.26)$$

For simplicity, we shall denote $U_{ij}^{(*)} = U_{ij}^{(*)}(t)$.

The limiter adopted here for the two dimensional formulation is described below:

$$U_{i+1/2, j}^- = U_{ij}^{(0)} + \widetilde{U}_{ij} = U_{ij}^{(0)} + \sum_{l=1}^{K} U_{ij}^{(l)} \Phi_l^{(ij)}(x_{i+1/2}, r_j), \quad (2.27)$$

$$U_{i-1/2, j}^+ = U_{ij}^{(0)} - \widetilde{\widetilde{U}}_{ij} = U_{ij}^{(0)} - \left(-\sum_{l=1}^{K} U_{ij}^{(l)} \Phi_l^{(ij)}(x_{i-1/2}, r_j) \right), \quad (2.28)$$

$$U_{i, j+1/2}^- = U_{ij}^{(0)} + \widetilde{U}_{ij} = U_{ij}^{(0)} + \sum_{l=1}^{K} U_{ij}^{(l)} \Phi_l^{(ij)}(x_i, r_{j+1/2}), \quad (2.29)$$

$$U_{i, j-1/2}^+ = U_{ij}^{(0)} - \widetilde{\widetilde{U}}_{ij} = U_{ij}^{(0)} - \left(-\sum_{l=1}^{K} U_{ij}^{(l)} \Phi_l^{(ij)}(x_i, r_{j-1/2}) \right). \quad (2.30)$$

For the "troubled cells", we reconstruct the polynomial solutions while retaining their cell averages. In other words, we will reconstruct the degrees of freedom, or the moments,

$U_{ij}^{(l)}$, $(l = 1, \ldots, K)$ for the "troubled cells" I_{ij} and retain only the cell averages $U_{ij}^{(0)}$ through the WENO reconstruction technique to be given below.

2.3. WENO reconstruction as limiters for the RKDG methods

For one dimensional cases, we summarize the procedure for reconstructing the moments $U_i^{(l)}$, $(l = 1, \ldots, k)$ for the "troubled cells" I_i by using the WENO reconstructions. The detailed frame work is given in [15,28].

Step 1. Given the small stencils S_n, $(n = 1, \ldots, m)$ and the bigger stencil $\Gamma = \bigcup_{n=1}^{m} S_n$, we construct the lower degree reconstruction polynomials $p_n(x)$, $(n = 1, \ldots, m)$ using the cell averages in the small stencils and a higher degree reconstruction polynomial $q(x)$ using the cell averages in the bigger stencil. At the Gaussian or Gauss–Lobatto quadrature points x_G, we can gain associated formulas precisely in [15,28].

Step 2. We find the combination coefficients, also called linear weights, denoted by γ_n, $(n = 1, \ldots, m)$, which satisfy: $q(x_G) = \sum_{n=1}^{m} \gamma_n p_n(x_G)$. Different quadrature points correspond to different linear weights.

Step 3. We compute the smoothness indicators β_n, $(n = 1, \ldots, m)$ [10,21] for stencils S_n, $(n = 1, \ldots, m)$. The smoothness indicators are the same as for the reconstruction of all Gaussian or Gauss–Lobatto points in the same cell, thus significantly reducing the computational cost.

Step 4. We compute the nonlinear weights ω_n, $(n = 1, \ldots, m)$ based on the smoothness indicators. Then the final WENO approximations at the quadrature points x_G are given by:

$$U(x_G, t) \approx \sum_{n=1}^{m} \omega_n p_n(x_G). \quad (2.31)$$

Step 5. We obtain the reconstructed moments based on the reconstructed point values $U(x_G, t)$ at the quadrature points x_G and a numerical integration:

$$U_i^{(l)}(t) \approx \frac{1}{\sum_G \sigma_G \left(\Phi_l^{(i)}(x_G) \right)^2} \sum_G \sigma_G U(x_G, t) \Phi_l^{(i)}(x_G), (l = 1, \ldots, k). \quad (2.32)$$

Here σ_G are the quadrature weights for different points x_G. The polynomial solution in this cell I_i is then obtained via $U^h(x, t) = \sum_{l=0}^{k} U_i^{(l)}(t) \Phi_l^{(i)}(x)$, for $x \in I_i$ with the reconstructed moments $U_i^{(l)}(t)$, $(l = 1, \ldots, k)$ and the original cell average $U_i^{(0)}(t)$.

Step 6. The semi-discrete scheme is then discretized in time by a TVD Runge–Kutta method [21].

Remarks 1. In this paper, the reconstructions are performed after each inner stage of the TVD Runge–Kutta method. We define the time-step size $\Delta t = \frac{CFL * h}{\max(u) + c}$ for all the examples in one dimension.

Remarks 2. For two dimensional cases, the reconstruction of moments $U_{ij}^{(l)}$, $(l = 1, \ldots, K)$ for the "troubled cells" I_{ij} is done with a "dimension-by-dimension" fashion like the steps for 1D as shown in [15] and thus omitted here.

2.4. Treatment of cavitation

As mentioned in Section 1, special treatment has to be made to suppress the numerical oscillations occurring in the region of cavitation. Firstly, we need to identify the cavitation mixture. Secondly, we need to construct a limiter procedure to suppress the numerical oscillations. Lastly, we want to faithfully obtain
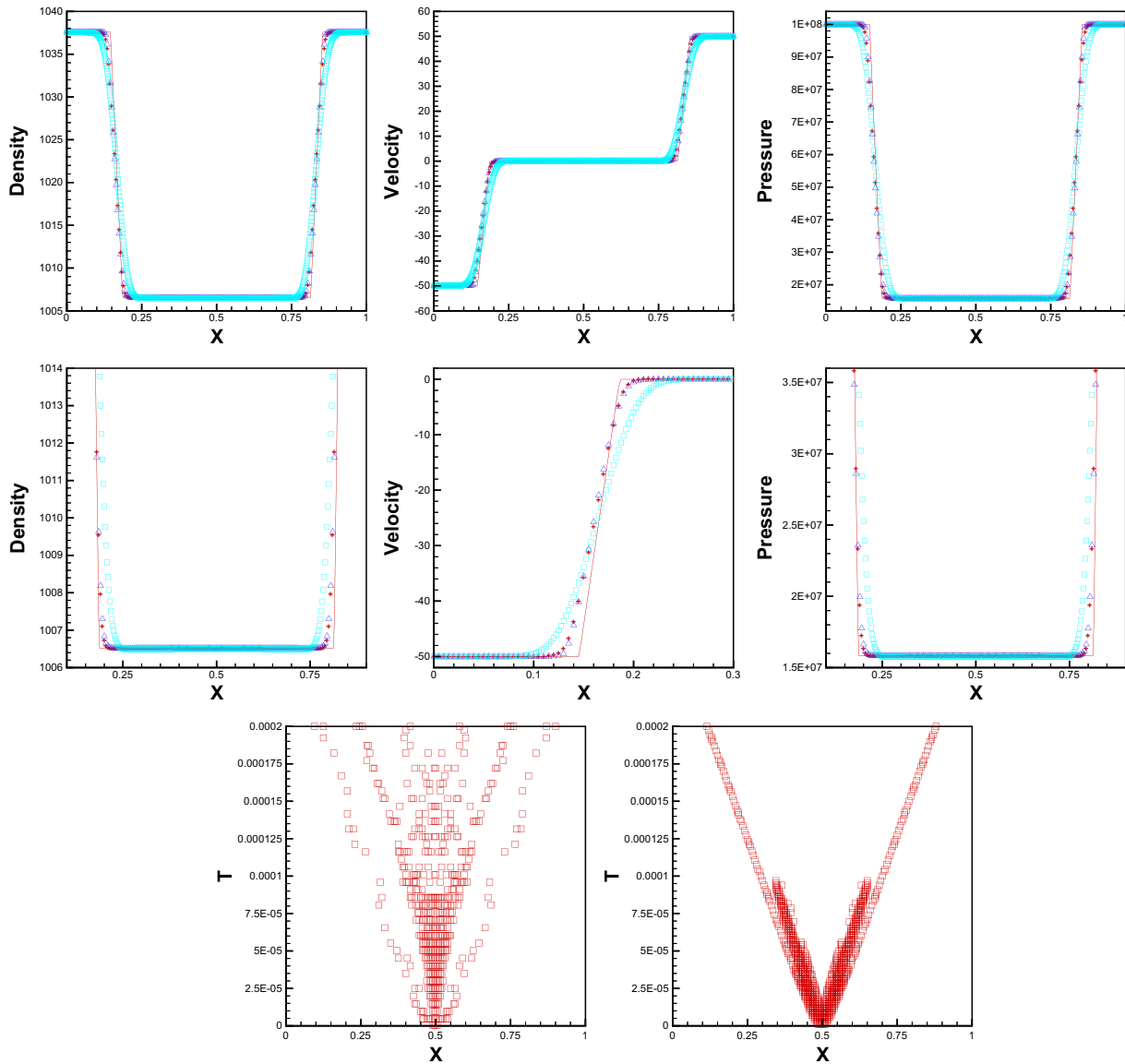
Fig. 1. The Example 3.1. From left to right and top to bottom: density; velocity; pressure; density zoom-in; velocity zoom-in; pressure zoom-in; the time history of the "troubled cells", squares denote cells which are identified as "troubled cells" subject to WENO limiting: WENO3-RKDG2 and WENO5-RKDG3. $t = 0.0002$. $M = 1$. Line: analytical solution; deltas: WENO3-RKDG2 solution, 200 cells; pluses: WENO5-RKDG3 solution, 200 cells; squares: MUSCL solution, 400 cells.

the flow state in the region of cavitation. Below is the summarized procedure of treating the region of cavitation.

Step 1. Identify the cavitation region. We treat the cavitation region as a "troubled" region and employ the TVB limiter shown in (2.24) as an indicator specially for the density by taking advantage of local flow physics, in which the density experiences a large jump across the cavitation interface (front). Of course, some of the single phase locations such as near a shock front or a contact discontinuity might be wrongly identified as cavitation cells. This misidentification does not cause any undesirable consequence as stated in **Step 3**.

Step 2. Carry out the WENO reconstruction for the identified "troubled cavitation cells" by following exactly the same steps listed in Section 2.3. With this step, the numerical oscillations occurring to the conservation variables in the cavitation region was found to be suppressed very well.

Step 3. Recover the cavitation flow state. With the reconstructed conservation variables, we compute the flow pressure and void fraction if necessary. In order to do so, we first assume that the "troubled cavitation cell" is a single phase cell (pure liquid) and compute the flow pressure with Tait's EOS. If the computed pressure is higher than the given saturated pressure, the "troubled cavitation cell" is wrongly identified and only exists as a single phase (pure liquid) cell, and the computed pressure is kept. If the computed pressure is lower than the given saturated pressure, the "troubled cavitation cell" is truly a cell located in the cavitation region, and the local pressure is recomputed using the cavitation EOS (2.14) together with void fraction calculated with (2.15).

Because the cavitation is modeled as a mixed one-fluid flow, we found that the WENO reconstruction as a limiter works very well to eliminate the numerical oscillation occurring in the cavitation
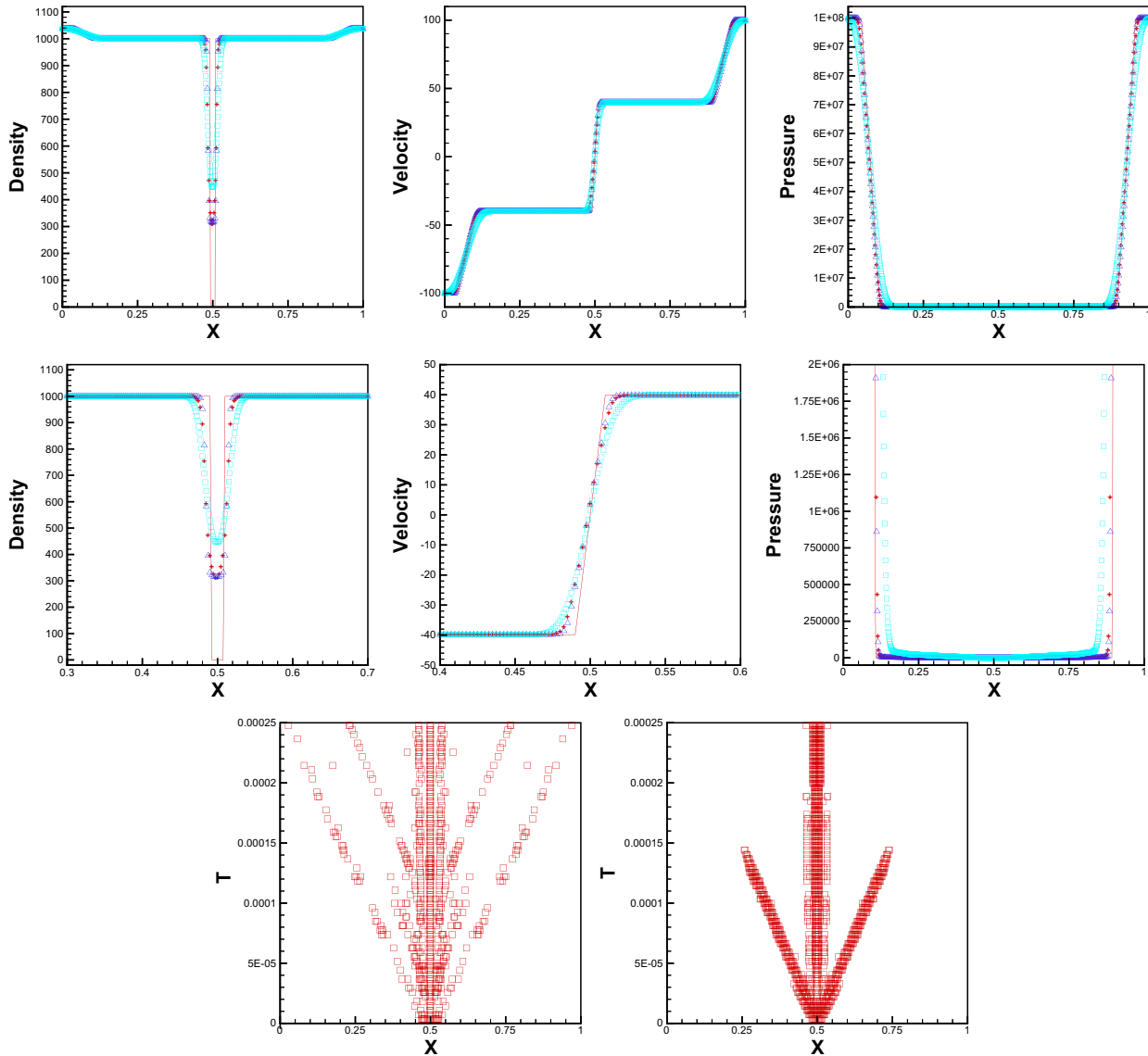
Fig. 2. The Example 3.2. From left to right and top to bottom: density; velocity; pressure; density zoom-in; velocity zoom-in; pressure zoom-in; the time history of the "troubled cells", squares denote cells which are identified as "troubled cells" subject to WENO limiting: WENO3-RKDG2 and WENO5-RKDG3. *t* = 0.00025. *M* = 1. Line: analytical solution; deltas: WENO3-RKDG2 solution, 400 cells; pluses: WENO5-RKDG3 solution, 400 cells; squares: MUSCL solution, 800 cells.

region. Although we have separately listed out the procedure of WENO reconstruction to the single phase flow and the cavitation flow, this procedure can be done simultaneously without much modification needed to the single phase code.

3. Numerical tests

Now, we present the results of numerical tests for several problems by the WENO3-RKDG2 and WENO5-RKDG3 schemes with isentropic one-fluid model described in Section 2. In this paper, we choose the CFL numbers to be 0.3 for WENO3-RKDG2 (where we have used the WENO3 schemes as limiters for the DG methods by using the second order version of the TVD Runge–Kutta method) schemes and 0.18 for WENO5-RKDG3 (employing the WENO5 schemes as limiters for the DG methods by using the third order version of the TVD Runge–Kutta method) schemes in one and two dimensions. The saturation vapor pressure is set at 62.5 Pa for the occurrence of cavitation, if any. In these tests, the units for the density, velocity, pressure, length and time are kg/m³, m/s, Pa, m and s, respectively. The main purpose of the examples

including cavitation and shock-cavitation interaction is to verify our proposed schemes in resolving the cavitating regions sharply without spurious oscillations.

Example 3.1. This is a case of one dimensional cavitating flow in an open tube in high pressure. It is a Riemann problem of two high pressure water streams moving with the same magnitude of velocity in the opposite direction away from the center of the tube. We consider the one dimensional Eq. (2.1) with initial conditions:

$$(\rho, u, p, N)^T = \begin{cases} (1000, -50, 10^8, 7.15)^T, & 0 \leqslant x \leqslant 0.5, \\ (1000, 50, 10^8, 7.15)^T, & 0.5 < x \leqslant 1. \end{cases} \quad (3.1)$$

Because the magnitude of initial two water streams' velocity are not so high, two centered rarefaction waves are generated and expands to the vicinity of the tube's center. In this way, we can get the analytical solution by solving a Riemann problem of double rarefaction waves. The computed density, velocity and pressure are plotted in Fig. 1 at *t* = 0.0002 using different numerical schemes together with the time history of the "troubled cells" with TVB constant of *M* = 1. (One of the other numerical
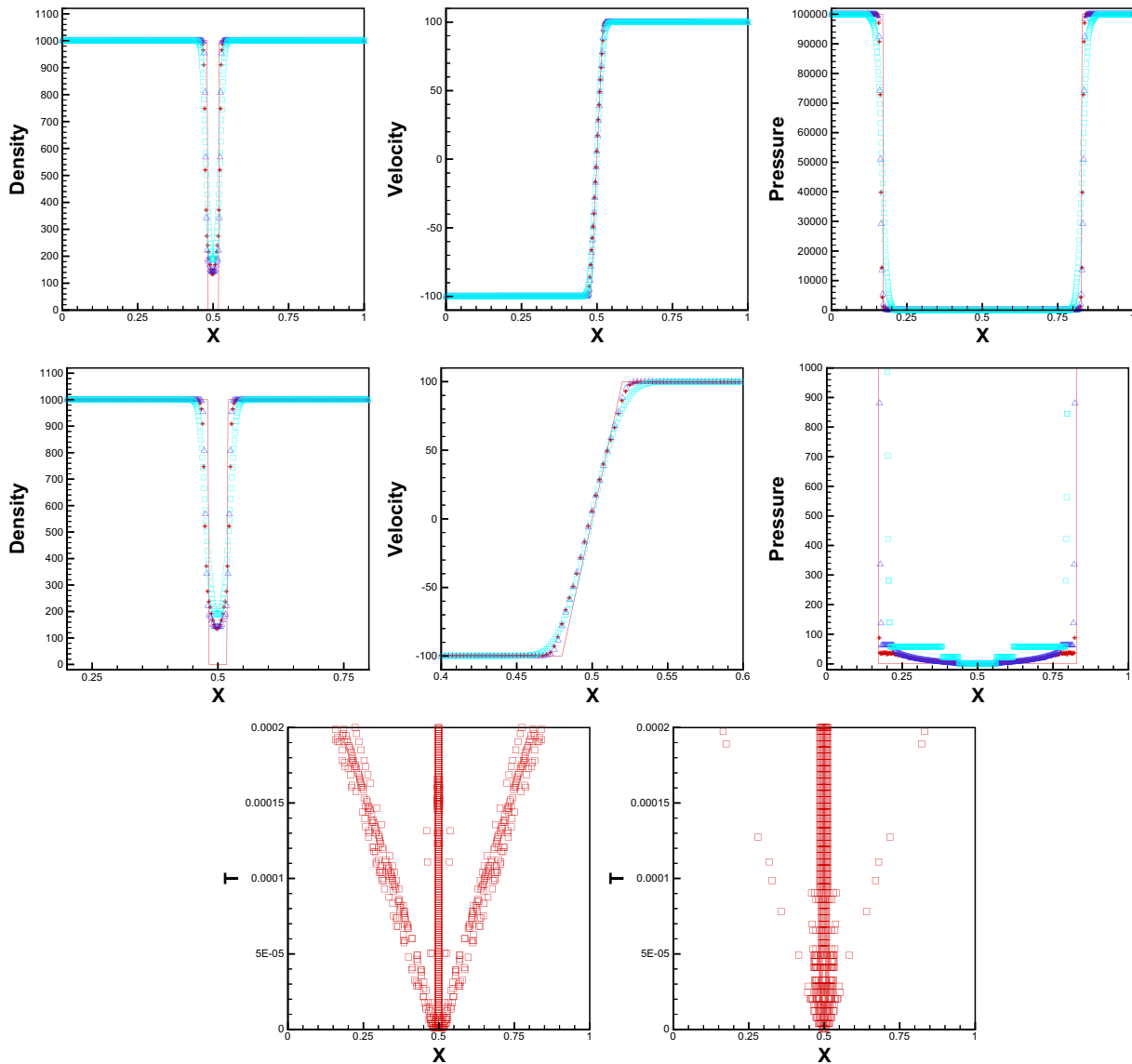
Fig. 3. The Example 3.3. From left to right and top to bottom: density; velocity; pressure; density zoom-in; velocity zoom-in; pressure zoom-in; the time history of the "troubled cells", squares denote cells which are identified as "troubled cells" subject to WENO limiting: WENO3-RKDG2 and WENO5-RKDG3. t = 0.0002. M = 1. Line: analytical solution; deltas: WENO3-RKDG2 solution, 400 cells; pluses: WENO5-RKDG3 solution, 400 cells; squares: MUSCL solution, 800 cells.

schemes selected is based on MUSCL-approach taken directly from [11] for comparison to the present WENO3-RKDG2 and WENO5-RKDG3 schemes.) The open boundary condition is used. We can see that the WENO3-RKDG2 and WENO5-RKDG3 scheme provide for lower quantity of density, a lesser smeared velocity profile and more accurate pressure level as compared to the MUSCL scheme vis-a-vis the analytical solution; the present schemes can provide the physical quantities at the transition more sharply. The time history of the "troubled cells" shows the reconstruction procedure is symmetrical and concentrated on the center region. Overall, the simulation results by the two present schemes though fairly comparable to the MUSCL scheme proposed in [11] have enabled sharper distribution profiles with high accuracy which are closer to the analysis.

Example 3.2. This is a case of one dimension cavitating flow in an open tube at higher initial velocity magnitude with initial conditions:

$$(\rho, u, p, N)^T = \begin{cases} (1000, -100, 10^8, 7.15)^T, & 0 \leqslant x \leqslant 0.5, \\ (1000, 100, 10^8, 7.15)^T, & 0.5 < x \leqslant 1. \end{cases} \quad (3.2)$$

The computed density, velocity and pressure are plotted in Fig. 2 at t = 0.00025 against the analytical solution for the different numerical schemes; the time history of the "troubled cells" with TVB constant of M = 1 is also provided. The open boundary condition is used. It is clear the WENO3-RKDG2 and WENO5-RKDG3 schemes can provide for a lower quantity of density, a sharper and less smeared velocity profile and more accurate pressure quantity in the cavitation region. It is interesting to note the WENO3-RKDG2 and WENO5-RKDG3 schemes have enabled the physical quantities of transition to be tracked relatively more sharply near the boundary of the cavitation region compared to the MUSCL-scheme although the number of the transition cells is less. The time history of the "troubled cells" shows the reconstruction procedure is symmetrical and concentrates on the cavitation region.
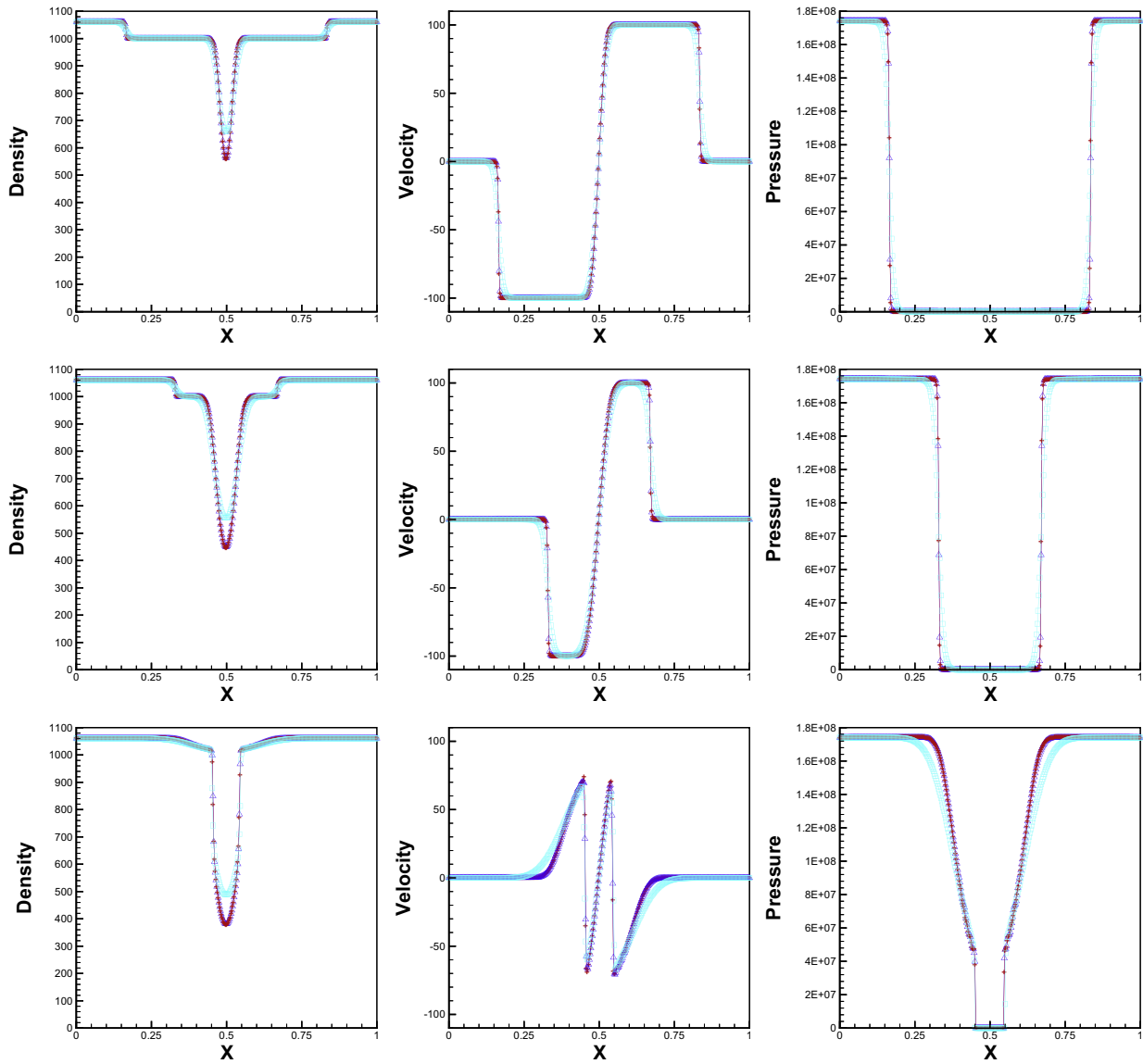
Fig. 4. The Example 3.4. From left to right: density; velocity; pressure. From top to bottom: $t = 0.0001$; $t = 0.0002$; $t = 0.0003$. $M = 1$. Line and deltas: WENO3-RKDG2 solution; line and pluses: WENO5-RKDG3 solution; line and squares: MUSCL solution. 400 cells.

Example 3.3. This is a case of one dimensional cavitating flow in an open tube at one atmosphere and is taken from [11]. The initial conditions are

$$(\rho, u, p, N)^T = \begin{cases} (1000, -100, 10^5, 7.15)^T, & 0 \leqslant x \leqslant 0.5, \\ (1000, 100, 10^5, 7.15)^T, & 0.5 < x \leqslant 1. \end{cases} \quad (3.3)$$

The computed density, velocity and pressure are plotted in Fig. 3 at $t = 0.0002$ against the analytical solution together with the time history of the "troubled cells" with TVB constant of $M = 1$. The open boundary condition is used. Again, it is found that the WENO3-RKDG2 and WENO5-RKDG3 schemes can provide for a lower quantity of density, a sharper and less smeared velocity profile and more accurate pressure quantity in the cavitation region as compared to the MUSCL scheme.

Example 3.4. We consider the Eq. (2.1) for one dimensional cavitating flow in a closed tube [11] with the following initial flow conditions
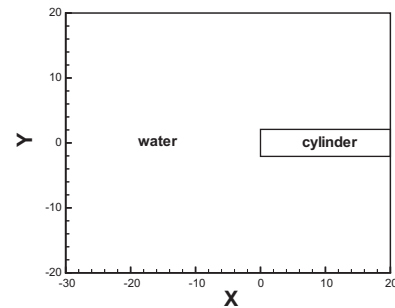
Fig. 5. The Example 3.5. Schematics of the computational domain.

$$(\rho, u, p, N)^T = \begin{cases} (1000, -100, 10^5, 7.15)^T, & 0 \leqslant x \leqslant 0.5, \\ (1000, 100, 10^5, 7.15)^T, & 0.5 < x \leqslant 1. \end{cases} \quad (3.4)$$
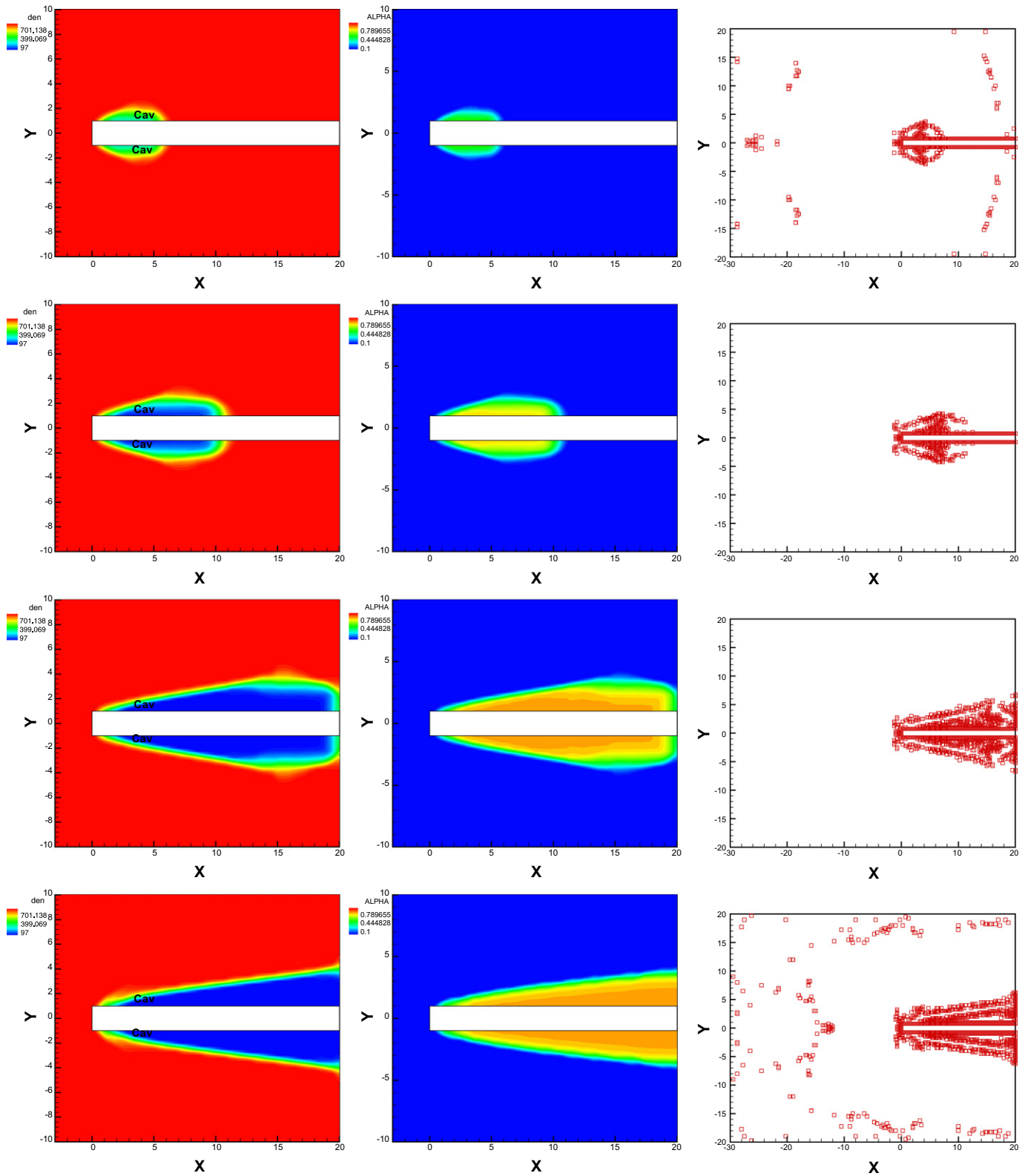
Fig. 6. The Example 3.5. From left to right: 30 equally spaced density contours from 97 to 973, density zoom-in, "Cav" indicates the cavitation region; 30 equally spaced void fraction α contours from 0.1 to 1.1, void fraction α zoom-in; the "troubled cells", squares denote cells which are identified as "troubled cells" subject to WENO limiting. From top to bottom: $t = 0.05$; $t = 0.1$; $t = 0.2$; $t = 0.25$. $M = 1$. WENO3-RKDG2 solution. 200×160 cells.

The main difference between this example and the previous three case-examples is that the two ends of the tube are closed and a shock created at each end moves towards the center and thus results in a shock-cavitation interaction. We set the two ends are reflective boundary conditions. The computed density, velocity and pressure are plotted at $t = 0.0001$, 0.0002, 0.0003 in Fig. 4. We can see the WENO3-RKDG2 and WENO5-RKDG3 schemes can provide for a lower quantity of density calculated,
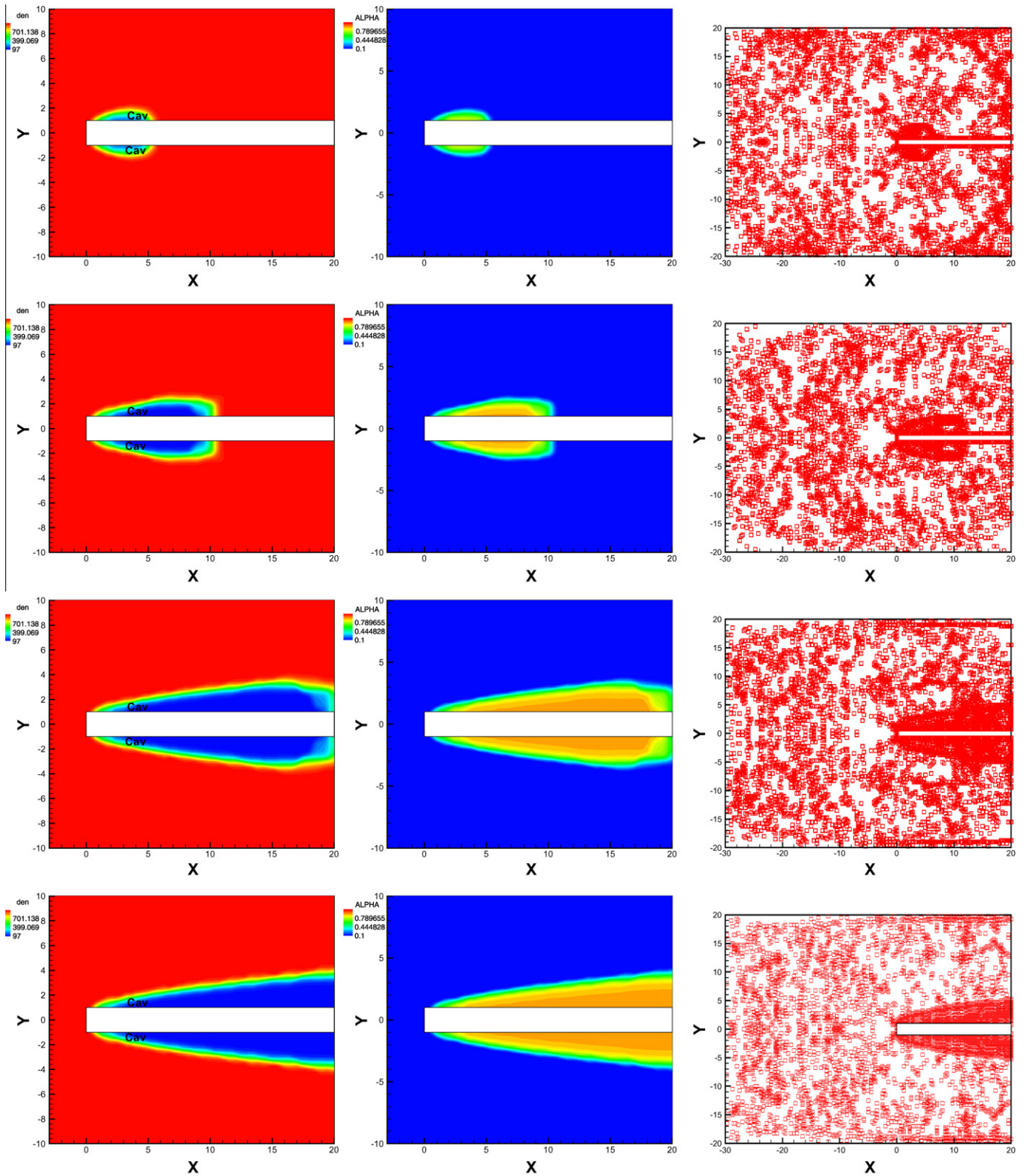
Fig. 7. The Example 3.5. From left to right: 30 equally spaced density contours from 97 to 973, density zoom-in, "Cav" indicates the cavitation region; 30 equally spaced void fraction α contours from 0.1 to 1.1, void fraction α zoom-in; the "troubled cells", squares denote cells which are identified as "troubled cells" subject to WENO limiting. From top to bottom: $t = 0.05$; $t = 0.1$; $t = 0.2$; $t = 0.25$. $M = 1$. WENO5-RKDG3 solution. 200×160 cells.

a sharper and less smeared velocity profile with higher magnitude reached, and can maintain the same pressure quantity near zero in the cavitation area. These, we reckoned are more accurate physical feature associated with the cavitation region (there is no analytical result for this case). Separately the computed time history of the "troubled cells" indicates symmetrical feature fairly similar to the previous case-examples (and not shown here).
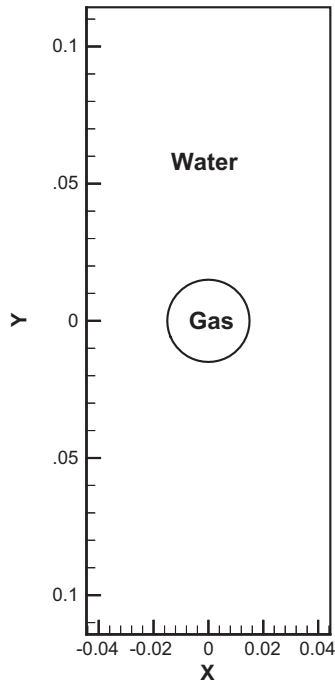
Fig. 8. The Example 3.6. Schematics of the computational domain.

Example 3.5. We use the two dimensional system (2.3). The initial flow conditions are

$$(\rho, u, v, p, N)^T = (1000, 100, 0, 10^5, 7.15)^T, \quad (x, y) \in [-30, 20] \times [-20, 20]. \quad (3.5)$$

There is a 2D (cylindrical) object given by $[0, 20] \times [-1, 1]$ in the computational region and placed in a much larger water medium measuring $[-30, 20] \times [-20, 20]$ with flow velocity from left to right. The schematic of the problem is provided in Fig. 5. The computed density, the "troubled cells" with TVB constant of $M = 1$ and the void fraction α are plotted at $t = 0.05, 0.1, 0.2, 0.25$ in Figs. 6 and

7. The inflow boundary condition is used on the left boundary and outflow boundary condition is used on the other three boundaries. On the object, reflective boundary condition is employed. As time progresses in the calculation, the pressure drops to below the saturated water vapor pressure at 62.5 Pa, a mixture of cavitation region is generated and can extend to envelop the whole object. We can see from the density figure that the cavitation region dimension in the y-direction becomes larger with further downstream. The value of the density increases from the surface of the cylinder to the free stream region both in the x- and y-directions. The computed result is oscillatory free for the density.

Example 3.6. A spherical underwater explosion in a rigid cylindrical container problem [11]. The diameter and the height of the cylinder are 0.0889 and 0.2286 m. The explosive gas sphere is located at the center of the cylinder full of water. The diameter of the gas sphere is 0.03 m. The initial pressure and density inside the gas sphere are 20,000 bar and 1770 kg/m³, and $\gamma = 2$ for the explosive gas. The problem is cast as a 2D cylindrical coordinate system (2.3). The p_{sat} is set to be 0.05 bar. The reflective boundary condition is used for the cylinder wall. The schematic of the problem is provided in Fig. 8. The computed pressure and the "troubled cells" with TVB constant of $M = 10$ at $t = 30 \, \mu s$, $60 \, \mu s$, $90 \, \mu s$, $120 \, \mu s$, and the pressure history at the center location of the side wall are plotted from Figs. 9–13, accordingly, for both the WENO3-RKDG2 and WENO5-RKDG3 solutions. The schemes show fairly similar results to that found in [11] with essentially the same physical flow dynamics. The peak value of the pressure at the center location of the wall shown in Fig. 13, however, exhibits a little higher value than that obtained in [11].

In essence, in our proposed approach, we have rebuilt the solutions in the "troubled cells" and retain the original high order accuracy of the RKDG methods. In this Example, it is clear that our approach can successfully capture the phenomena of the underwater shock reflected from the cylinder wall, the interaction of the reflected shock and the expanding gas bubble interface, the shock-shock interaction and the shock-cavitation interaction.
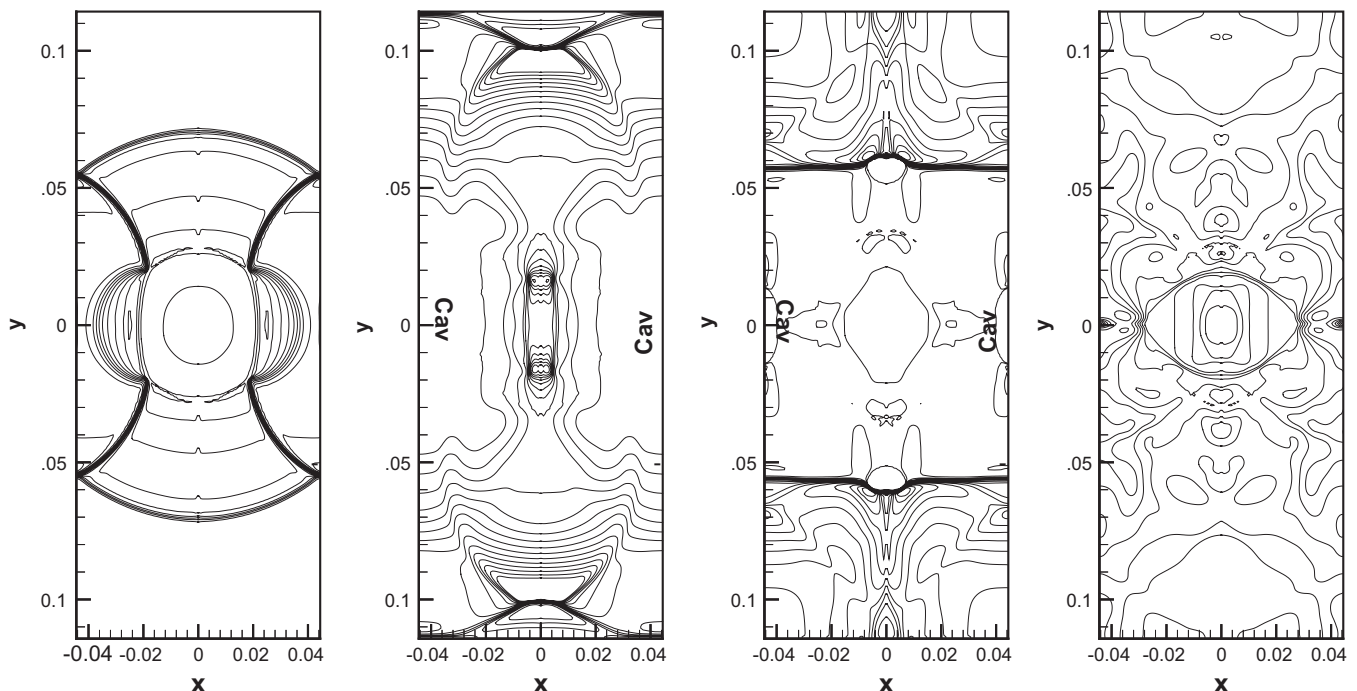
Fig. 9. The Example 3.6. A 15 equally spaced pressure contours from 343 to 5141, "Cav" indicates the cavitation region. From left to right: $t = 30 \, \mu s$, $60 \, \mu s$, $90 \, \mu s$, $120 \, \mu s$. $M = 10$. WENO3-RKDG2 solution. 140×360 cells.
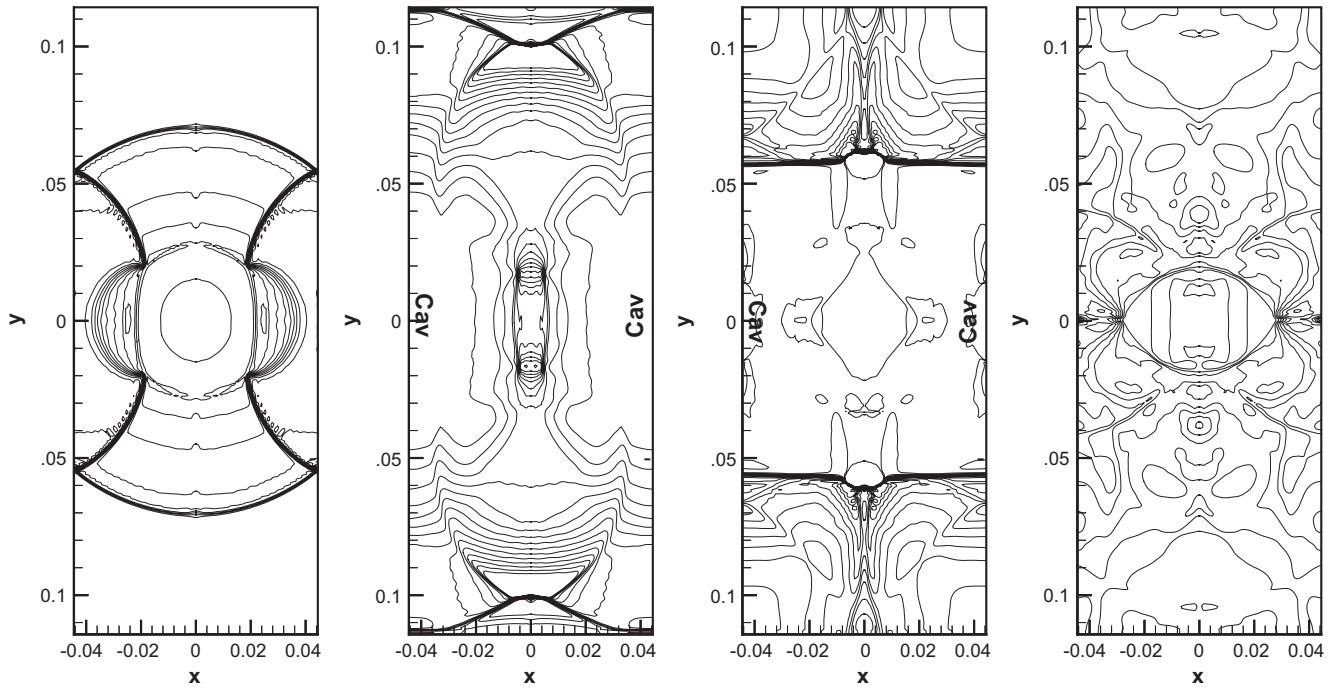
Fig. 10. The Example 3.6. A 15 equally spaced pressure contours from 343 to 5141, "Cav" indicates the cavitation region. From left to right: *t* = 30 μs, 60 μs, 90 μs, 120 μs. *M* = 10. WENO5-RKDG3 solution. 140 × 360 cells.
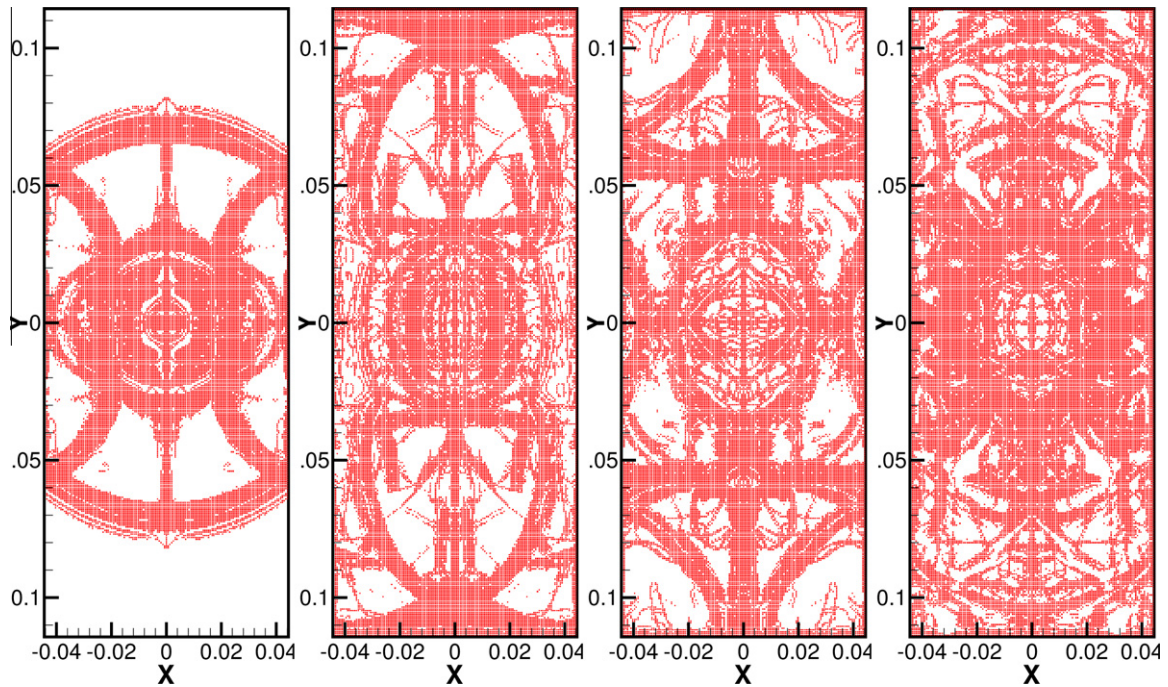
Fig. 11. The Example 3.6. The "troubled cells", squares denote cells which are identified as "troubled cells" subject to WENO limiting. From left to right: *t* = 30 μs, 60 μs, 90 μs, 120 μs. *M* = 10. WENO3-RKDG2 solution. 140 × 360 cells.

4. Concluding remarks

We have developed the RKDG methods with the WENO reconstruction as limiters to solve for the unsteady cavitating flow in one and two dimensions with the isentropic one-fluid model. To treat the numerical oscillation occurring in the cavitation region, the cavitation region is reckoned as "troubled cells". For the solution solvers, the main idea is to first identify the "troubled cells" subject to the WENO limiting, which uses a TVB minmod-type limiter to be followed by reconstruction of the polynomial solutions inside the "troubled cells" via WENO reconstructions of conservation variables. Numerical results in one and two dimensions are provided
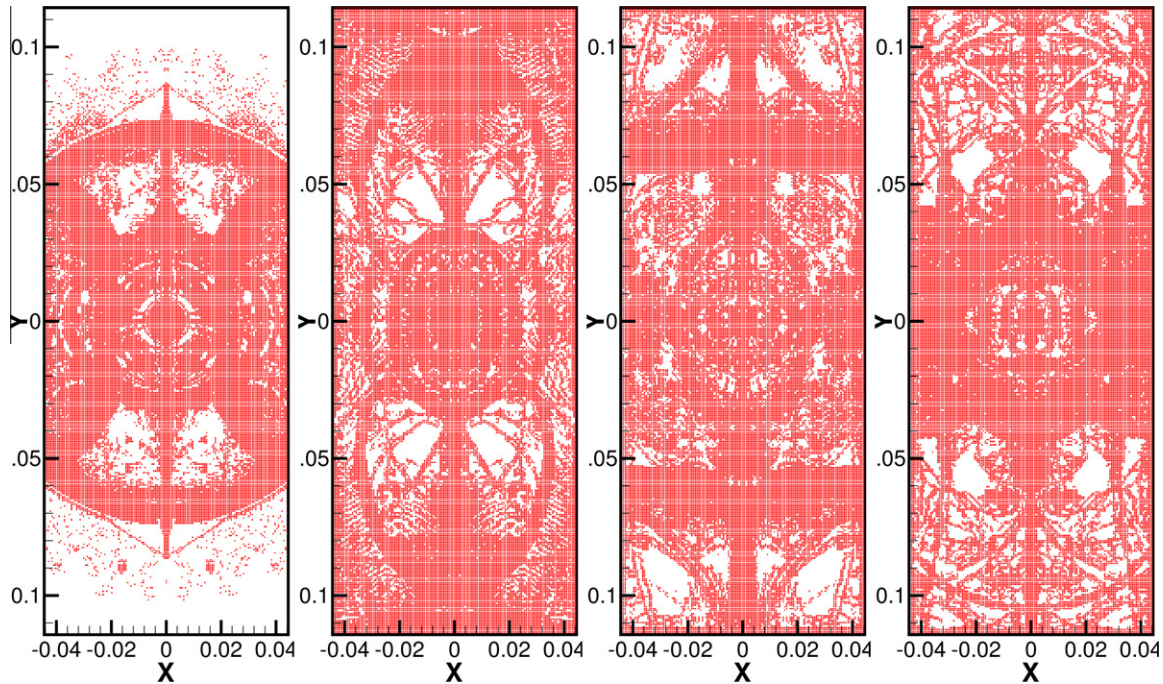
Fig. 12. The Example 3.6. The "troubled cells", squares denote cells which are identified as "troubled cells" subject to WENO limiting. From left to right: $t = 30$ µs, 60 µs, 90 µs, 120 µs. $M = 10$. WENO5-RKDG3 solution. 140×360 cells.

Fig. 13. The Example 3.6. Pressure history at the center location of the side wall. $M = 10$. Line and deltas: WENO3-RKDG2 solution; line and pluses: WENO5-RKDG3 solution. 140×360 cells.

to show that these methods are stable and robust subject to a wide range of initial conditions. The proposed methods have been found to be able to provide accurate and sharp vapor–liquid boundary locations and still with reasonable resolutions for the respective pure liquid and vapor–liquid mixture regions and very well limited oscillations.

Acknowledgements

References

[1] Biswas R, Devine KD, Flaherty J. Parallel, adaptive finite element methods for conservation laws. Appl Numer Math 1994;14:255–83.

[2] Brennen CE. Cavitation and bubble dynamics. Oxford: Oxford University Press; 1995.

[3] Burbeau A, Sagaut P, Bruneau CH. A problem-independent limiter for high-order Runge–Kutta discontinuous Galerkin methods. J Comput Phys 2001;169:111–50.

[4] Cockburn B, Hou S, Shu CW. The Runge-Kutta local projection discontinuous Galerkin finite element method for conservation laws. IV: The multidimensional case. Math Comput 1990;54:545–81.

[5] Cockburn B, Lin SY, Shu CW. TVB Runge–Kutta local projection discontinuous Galerkin finite element method for conservation laws. III: one dimensional systems. J Comput Phys 1989;84:90–113.

[6] Cockburn B, Shu CW. TVB Runge–Kutta local projection discontinuous Galerkin finite element method for conservation laws. II: General framework. Math Comput 1989;52:411–35.

[7] Cockburn B, Shu CW. The Runge–Kutta local projection P1-discontinuous Galerkin finite element method for scalar conservation laws. Math Model Numer Anal (M2AN) 1991;25:337–61.

[8] Cockburn B, Shu CW. The Runge-Kutta discontinuous Galerkin method for conservation laws. V: Multidimensional systems. J Comput Phys 1998;141:199–224.

[9] Fedkiw RP, Aslam T, Merriman B, Osher S. A non-oscillatory Eulerian approach to interfaces in multimaterial flows (the ghost fluid method). J Comput Phys 1999;152:457–92.

[10] Jiang GS, Shu CW. Efficient implementation of weighted ENO schemes. J Comput Phys 1996;126:202–28.

[11] Liu TG, Khoo BC, Xie WF. Isentropic one-fluid modelling of unsteady cavitating flow. J Comput Phys 2004;201:80–108.

[12] Liu TG, Khoo BC, Yeo KS. The simulation of compressible multi-medium flow. Part I: A new methodology with applications to 1D gas–gas and gas–water cases. Comput Fluids 2001;30:291–314.

[13] Luo H, Baum JD, Lohner R. A Hermite WENO-based limiter for discontinuous Galerkin method on unstructured grids. J Comput Phys 2007;225:686–713.

[14] Qiu J, Shu CW. Hermite WENO schemes and their application as limiters for Runge–Kutta discontinuous Galerkin method: one dimensional case. J Comput Phys 2004;193:115–35.

[15] Qiu J, Shu CW. Runge–Kutta discontinuous Galerkin method using WENO limiters. SIAM J Sci Comput 2005;26:907–29.

[16] Qiu J, Shu CW. Hermite WENO schemes and their application as limiters for Runge–Kutta discontinuous Galerkin method. II: Two-dimensional case. Comput Fluids 2005;34:642–63.

[17] Reed WH, Hill TR. Triangular mesh methods for neutron transport equation. Tech Report LA-UR-73-479. Los Alamos Scientific Laboratory; 1973.

[18] Saurel R, Abgrall R. A multiphase Godunov method for compressible multifluid and multiphase flows. J Comput Phys 1999;150:425–67.

[19] Schmidt DP, Rutland CJ, Corradini ML. A fully compressible, two-dimensional model of small, high speed, cavitating nozzles. Atomiz Sprays 1999;9:255–76.

[20] Shu CW. TVB uniformly high-order schemes for conservation laws. Math Comput 1987;49:105–21.

[21] Shu CW. Essentially non-oscillatory and weighted essentially non-oscillatory schemes for hyperbolic conservation laws. In: Quarteroni A, editor. Advanced numerical approximation of nonlinear hyperbolic equations. Lecture notes in mathematics. CIME subseries. ICASE Report 97-65. Berlin/New York: Springer-Verlag; 1997.

[22] Shu CW, Osher S. Efficient implementation of essentially non-oscillatory shock capturing schemes. J Comput Phys 1988;77:439–71.

[23] Tang HS, Huang D. A second-order accurate capturing scheme for 1D inviscid flows of gas and water with vacuum zones. J Comput Phys 1996;128:301–18.

[24] Wallis GB. One-dimensional two-phase flow. New York: McGraw-Hill; 1969.

[25] Xie WF, Liu TG, Khoo BC. Application of a one-fluid model for large scale homogeneous unsteady cavitation: the modified Schmidt model. Comput Fluids 2006;35:1177–92.

[26] Zhu J, Qiu J. Hermite WENO schemes and their application as limiters for Runge–Kutta discontinuous Galerkin method. III: Unstructured meshes. J Sci Comput 2009;39:293–321.

[27] Zhu J, Qiu J. Local DG method using WENO type limiters for convection–diffusion problems. J Comput Phys 2011;230:4353–75.

[28] Zhu J, Qiu J, Liu TG, Khoo BC. RKDG methods with WENO type limiters and conservative interfacial procedure for one-dimensional compressible multi-medium flow simulations. Appl Numer Math 2011;61:554–80.

[29] Zhu J, Qiu J, Shu CW, Dumbser M. Runge–Kutta discontinuous Galerkin method using WENO limiters. II: Unstructured meshes. J Comput Phys 2008;227:4330–53.